Master Sciences de la Matière
École normale supérieure de Lyon
Université Claude Bernard Lyon 1

Notes - Spring 2017
Yann-Edwin KETA
M1 Physique

Numerical analysis of jamming criticality for spheroidal particles

Abstract: *We present here the methods and models we have developed or adapted from the study of static or sheared packings of spheres to the study of sheared packings of spheroids. These allow us to investigate the critical behaviours observed at the jamming transition and the other behaviours observed near the rheological transition of packings of soft-core frictionless spheroids. We show that our models give results in good accordance with existing literature and point out interesting phenomena which could give new insights into the jamming transition.*

Project supervised by:

Peter OLSSON
peter.olsson@tp.umu.se
tél. +46 90 7865046
Institutionen för fysik
Umeå universitet
SE-90187 Umeå, Sweden
http://physics.umu.se/

Contents

Introduction

Granular materials are ubiquitous in nature and are the second-most manipulated material in industry [1]. These are non-thermal systems, *i.e.* their kinetic energy vanishes in absence of an external drive. Despite their relative simplicity, they exhibit a wide range of interesting – even fascinating – behaviours [2].

Granular matter can show either liquid-like or solid-like properties under different experimental conditions. This transition from a flowing state to a rigid state is known as the *jamming transition*, and has been the subject of much recent work. Understanding why and how these materials transition from one of this state to the other is indeed of great theoretical interest, *e.g.* understanding the mechanisms which govern jamming in athermal macroscopic systems may help us to understand how supercooled liquid freeze into a frozen glass [3].

Numerical shearing simulations of non-rotating frictionless soft-core disks have been proven particularly efficient to study the jamming transition [4, 5]. Our present report aims to present the methods which have been employed in such studies and to show how they can and have been modified and enriched to study more general rotating frictionless soft-core spheroids (*ie.* ellipsoids of revolution), both prolate – elongated – and oblate – flattened.

Computer programs were written in MATLAB language for evaluation of the methods then in C language for performance (speed of execution). All the code developed specifically for this project is available on GitHub, in the repository yketa/Umea-universitet---Spring-2017---code. Simulations with 64 and 1024 particles were run on 1 and 4 cores respectively on computers provided by the Department of Physics at Umeå University. Simulations with 16384 particles were run on 12 cores on the supercomputer provided by the Swedish National Infrastructure for Computing (SNIC) at High Performance Computing Center North (HPC2N).

This report is organised as follows. In chapter 1, we thoroughly describe the jamming transition, as well as the models and methods we have used, modified and improved. In chapter 2 we present and discuss the numerical results we have obtained so far. In appendix A we explicitly calculate the harmonic elastic force between two ellipsoids.

1 | Jamming

Many recent works have studied the properties of the jamming transition for packings of 2D and 3D soft- and hard-core spherical particles. Our goal here is to investigate how these properties are affected when considering spheroids.

We will first introduce the jamming transition and the models and methods that have been involved to study this transition for spheres and then present the modifications we have brought to these in order to study rotating spheroids.

1.1 Jamming transition

1.1.1 Phenomenon

A few decades ago, little was still known about granular materials. According to Pierre-Gilles de Gennes, "granular matter in 1998 [was] at the level of solid state physics in 1930." [6] Yet, these materials are of great theoretical interest in the domain of statistical physics [7].

What has been observed is that granular materials develop a yield stress in a disordered state [8] – or a stress relaxation time which exceeds a reasonable experimental time – upon increasing the packing fraction ϕ above a critical value ϕ_J. At low ϕ, each particle can move independently of its neighbours while at high ϕ the particles can not avoid each other, resulting in a bulk modulus since the pressure increases upon compression. This phenomenon is called jamming and corresponds to a transition from a flowing liquid-like state to an amorphous rigid solid state.

Jamming is encountered everywhere, whether it is unintended – *e.g.*, grains and beans jam in hoppers [9–11], cars jam on the highway [12] – or purposefully put into practice in engineering applications – *e.g.*, to easily, efficiently and reliably hold objects [13, 14].

The phenomenon is also present in other systems with other control parameters [15]. Foams jam upon decreasing the applied shear stress and supercooled liquids jam upon decreasing the temperature – the latter phenomenon being already known as the glass transition from a flowing liquid to a frozen glass.

These observations led Liu and Nagel to hypothesise that they are controlled by the same mechanisms [3], and thus to summarise them in a phase diagram [8] which axis are the aforementioned parameters: temperature T, shear stress σ and packing fraction ϕ (figure 1.1). The surface below which states are jammed corresponds to the points for which the system behaves like a solid on any experimental time scale and the point J is meant to correspond to the packing fraction ϕ_J at which the system at $T = 0$ and $\sigma = 0$ jam in the thermodynamic limit (infinite system, *i.e.*, $N \to +\infty$).

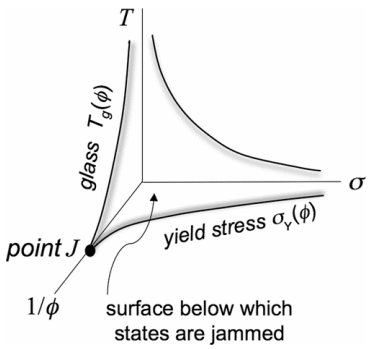

Figure 1.1: *source:* [5]

Defining what is exactly a "jammed system" is a problem of great mathematical and physical interest [16, 17], in particular it has finally allowed physicists to replace the concept of random close packing (RCP) with the more rigorous and precise concept of maximally random jammed (MRJ) state [18]. We will however set aside these considerations to rather focus on the critical behaviours (parts 1.1.2 and 1.1.3) observed at the transition to such a state.

1.1.2 Critical behaviour

In the vicinity of J, we have that the shear viscosity $\eta \equiv \sigma/\dot{\gamma}$ – with σ the shear stress and $\dot{\gamma}$ the shear strain rate, – or equivalently the pressure viscosity $\eta_p \equiv p/\dot{\gamma}$ – with p the pressure, – and a correlation length scale ξ diverge as

$$\begin{aligned} \eta, \eta_p &\underset{\phi \to \phi_J}{\sim} (\phi_J - \phi)^{-\beta} \\ \xi &\underset{\phi \to \phi_J}{\sim} (\phi_J - \phi)^{-\nu} \end{aligned} \tag{1.1}$$

for soft-core particles in the limit $\dot{\gamma} \to 0$ [4, 19] and for hard-core particles [20].

Using η_p rather than η has been proven to reduce errors due to necessary corrections to scaling [19]. Moreover, we have to keep in mind that equation 1.1 holds only very close to ϕ_J. Since the macroscopic friction coefficient $\mu \equiv \eta/\eta_p$ has a strong ϕ-dependence, corrections may have to be added to the scaling for larger packing fractions intervals [19, 21]. Please refer to part 1.3 for more details on the scaling methods.

This power-law divergence of the transport coefficient and of a correlation length scale are reminiscent of the behaviour near a critical point [19, 22, 23] of a second-order continuous phase transition.

For frictional particles, it has been shown that the jamming transition was discontinuous [24]. However, equation 1.1, which has been well demonstrated for frictionless particles, can also be applied to frictional particles by introducing a fictitious critical density, somewhat higher than the density at which the system develops a yield stress.

1.1.3 Relaxation time

For a packing of soft-core particles at a density $\phi < \phi_J$ in the thermodynamic limit $N \to +\infty$, the state of minimum energy will always be a state where the particles do not overlap, therefore a state of zero energy and zero pressure. When one applies a constant shear strain rate to such a system, the particles overlap and the energy becomes non-zero. One can then be interested in the decay of the energy and the pressure when the shearing ceases.

Authors of [21] studied this decay for systems of soft-core disks with harmonic elastic interactions (see part 1.4) at constant shear strain rate. What they have observed is that after a short transient time, the pressure decays exponentially to zero with a characteristic time scale $\tau(\phi, \dot{\gamma})$

$$\boxed{p(t) \sim \exp\left(-t/\tau(\phi, \dot{\gamma})\right)} \tag{1.2}$$

which they called the *relaxation time*. This relaxation time increases with increasing initial shear strain rate $\dot{\gamma}$ for a given ϕ and diverges as ϕ approaches ϕ_J from below.

Another relevant time scale presented by the authors is the *dissipation time* $\tau_{\text{diss}}(\phi, \dot{\gamma})$, which represents the initial decay rate of the energy. It is obtained by taking the ratio of the energy E by the dissipated power P_{diss}. If the system is steadily sheared, then P_{diss} equals the input power $P_{\text{in}} \sim \sigma\dot{\gamma}$ with σ the shear stress. Therefore, $\tau_{\text{diss}}(\phi, \dot{\gamma}) \sim E/\sigma\dot{\gamma}$.

Since that, for harmonic elastic interactions, we have $p \sim \delta$ and $E \sim \delta^2$ with δ the overlap, we then expect the energy to decay exponentially with a characteristic time scale $\tau(\phi, \dot{\gamma})/2$. In consequence, the authors chose

$$\boxed{\tau_{\text{diss}}(\phi, \dot{\gamma}) = 2\frac{E}{\sigma\dot{\gamma}}} \tag{1.3}$$

for this time scale to be compared with $\tau(\phi, \dot{\gamma})$. Contrarily to the relaxation time, the dissipation time decreases with increasing initial shear strain rate $\dot{\gamma}$, but also diverges as ϕ approaches ϕ_J from below.

Indeed, if we notice that

$$\tau_{\text{diss}} = 2\frac{E}{\sigma\dot{\gamma}} \sim \frac{E/\dot{\gamma}^2}{\sigma/\dot{\gamma}} \sim \frac{(p/\dot{\gamma})^2}{\sigma/\dot{\gamma}} \sim \frac{\eta_p^2}{\eta}$$

we can directly infer from equation 1.1 that

$$\boxed{\tau_{\text{diss}} \underset{\phi\to\phi_J}{\sim} (\phi_J - \phi)^{-\beta}} \tag{1.4}$$

therefore, the dissipation time diverges with the same exponent as the viscosity and its pressure equivalent.

Authors of [21] finally showed that in the limit of low initial shear strain rate $\dot{\gamma} \to 0$, the relaxation time and the dissipation time behave essentially the same close to ϕ_J

$$\tau \underset{\substack{\dot{\gamma}\to 0 \\ \phi\to\phi_J}}{\sim} \tau_{\text{diss}} \tag{1.5}$$

therefore the relaxation time also diverges with the critical exponent β.

We emphasise that equations 1.4 and 1.5 give, in addition to the study of the quantities in equation 1.1, a way to determine the critical exponent associated with the divergence of the viscosity at the jamming transition.

It was then suggested that τ may be a fundamental quantity which controls the overlap $\delta/\dot{\gamma}$ and thus would be behind the divergence of the transport coefficients.

1.1.4 Orientational ordering

Considering non-spherical particles breaks down the isotropy of the rotation phase space. Therefore one can expect that, near the jamming transition, a system of ellipsoidal particles would develop a significant orientational ordering.

Nonetheless, it has been suggested that packings of ellipsoidal particles showed no such ordering at jamming in static simulations [25] but, since shearing breaks the isotropy of space, one can still hypothesise that such a phenomenon is to be expected in shearing simulations.

1.1.5 Finite-size effects

For a finite number N of particles, the system will jam at a packing fraction ϕ somewhat below ϕ_J because there is always a finite probability to find a configuration with a force chain spanning the width of the system, causing the system to jam.

When shearing a packing of particles the system explores an increasing region of configuration space, it will thus eventually find a configuration causing it to jam. The statistical weight of these configurations, in addition to the time required for the system to jam, decreases as one decreases the packing fraction ϕ or increases the number of particle N. Therefore, in the limit of an infinite system $N \to +\infty$, it is expected that the system jam in a finite time only for $\phi \geq \phi_J$ [4].

1.2 Methods

1.2.1 Jamming transition

Many numerical methods have been used to study the jamming of a system of spherical particles:

- Most of them consist of evaluating and studying the proportion of jammed states as a function of the density and infer from these data the jamming packing fraction. What distinguishes the methods is then the way the system is prepared:
  - Relaxations from initially random states [5, 23]. A system corresponding to a completely random state ($T = +\infty$) is cooled by using energy minimisation techniques.

  - Quasistatic shearing [23]. A system of which the energy has been initially minimised is gradually sheared, with energy minimisation steps between each increment of the shear strain.
  - Compression [26].

- Other methods are based on the shearing at constant shear rate of a given system [4], which can be performed using Lees-Edwards periodic boundary conditions [27, 28]. From the assumption of a critical behaviour of the mechanical properties (*e.g.*, pressure, shear modulus) near the jamming point J, the scaling analysis of the behaviour of the system enables one to infer the jamming packing fraction and the critical exponents.

However, there appears to have little agreement in the values for the jamming density and of the critical exponents found in the literature. This is thought to be caused by the neglect of corrections to scaling in these papers [19]. Moreover, in relaxation and compression protocols, particles tend to order themselves into clusters. This leads to values of the jamming density which are dependent of the way the samples were prepared and treated – a dependence which is often to be expected when studying granular materials [29, 30]. Some authors suggested that, since ϕ_J was history-dependent, the point J may be ill-defined, even when clustering plays no role [26].

We can note that, to avoid crystallisation, most simulations involve polydispersity [26].

On the contrary, the process of shearing – no matter how slow – breaks the clustering at the origin of varying and higher than expected values of ϕ_J. It has then been showed that quasistatic shearing protocols lead to an unique – well-defined – value of the jamming density ϕ_J, corresponding to the jamming density for shearing simulations in the limit of vanishing shear strain rate, which does not depend on the initial configuration or the details of the shearing protocol [5].

It has then been proposed to study jamming in the $(1/\phi, T, \dot{\gamma})$ phase space – where $\dot{\gamma}$ is the shear strain rate – where J would be unique. In such a phase space, the $(1/\phi, T)$ plane at $\dot{\gamma} \to 0$ corresponds to the plane of quasistatically sheared steady states.

1.2.2 Relaxation time

To study the relaxation time $\tau(\phi, \dot{\gamma})$ of a system of soft-core particles, the authors of [21] made use of a 2-stage process. First, the system is driven at steady shear with the constant shear strain rate $\dot{\gamma}$. Then, the shearing is stopped but the dynamics is continued until the system relaxes down to a minimum energy.

1.2.3 Soft- to hard-core mapping

Shearing simulations are more or less easily conducted with soft-core particles. We can be interested to know how the data from these simulation can be used to study the rheological behaviour of packings of hard-core particles near the jamming transition.

We can find in [20] a method to map soft-core particles at a given packing fraction ϕ and shear strain rate $\dot{\gamma}$ to equivalent hard-core particles at a lesser packing fraction ϕ_{eff} such as

$$\begin{aligned} \eta_p^s(\phi, \dot{\gamma}) &= \eta_p^s(\phi_{\text{eff}}, \dot{\gamma} \to 0) \\ \eta_p^h(\phi_{\text{eff}}) \equiv \eta_p^s(\phi_{\text{eff}}, \dot{\gamma} \to 0) &\underset{\phi_{\text{eff}} \to \phi_J}{\sim} (\phi_J - \phi_{\text{eff}})^{-\beta} \end{aligned} \tag{1.6}$$

according to equation 1.1. We denoted η_p^s and η_p^h are the pressure equivalents of viscosity for packings of soft- and hard-core particles respectively.

This mapping is done by assuming that ϕ_{eff} is determined by the extent of particle overlaps, measured by the average energy per particle $E(\phi, \dot{\gamma})$. Authors of [20] then proposed the following relation

$$\phi_{\text{eff}}(\phi, \dot{\gamma}) = \phi - h(E(\phi, \dot{\gamma})) \tag{1.7}$$

where h can be determined asymptotically close to ϕ_J.

We can first notice that there is no distinction between soft-core and hard-core particles in a system where the particles do not overlap. In such a system, the average energy per particle equals to 0, therefore we must have

$$h(0) = 0 \tag{1.8}$$

In a jammed system – *i.e.*, $\phi \geq \phi_J$ – of soft-core particles, particles have no choice but to overlap leading to $p > 0$ even as $\dot{\gamma} \to 0$, and then $\eta_p^s(\phi \geq \phi_J, \dot{\gamma} \to 0) \to +\infty$. In consequence, according to equation 1.6, we must have $\eta_p^h(\phi_{\text{eff}}) \to +\infty$, which is only achieved for a system of hard-core particles at $\phi_{\text{eff}} = \phi_J$, therefore

$$\phi_{\text{eff}}(\phi \geq \phi_J, \dot{\gamma} \to 0) = \phi_J \tag{1.9}$$

From equations 1.7 and 1.9, we have that

$$\phi_{\text{eff}}(\phi \geq \phi_J, \dot{\gamma} \to 0) = \phi - h(E(\phi, \dot{\gamma} \to 0)) = \phi_J \Rightarrow h(E(\phi, \dot{\gamma} \to 0)) = \phi - \phi_J$$

and, since $E(\phi, \dot{\gamma} \to 0)$ vanishes algebraically close to ϕ_J, we can write

$$\begin{aligned} E(\phi, \dot{\gamma} \to 0) \underset{\phi \to \phi_J}{\sim} (\phi - \phi_J)^{y_E} &\Leftrightarrow E(\phi, \dot{\gamma} \to 0)^{1/y_E} \underset{\phi \to \phi_J}{\sim} \phi - \phi_J \\ &\Rightarrow E(\phi, \dot{\gamma} \to 0)^{1/y_E} \underset{\phi \to \phi_J}{\sim} h(E(\phi, \dot{\gamma} \to 0)) \\ &\Rightarrow X^{1/y_E} \underset{X \to 0}{\sim} h(X) \end{aligned}$$

where the latter equivalence can be applied to $E(\phi, \dot{\gamma})$ in the vicinity of ϕ_J, therefore

$$\boxed{\phi_{\text{eff}}(\phi, \dot{\gamma}) \underset{\phi \to \phi_J}{=} \phi - cE(\phi, \dot{\gamma})^{1/y_E}} \tag{1.10}$$

with c a constant.

1.3 Scaling analysis

1.3.1 Scaling assumption

1.3.1.1 Principle

According to the discussions of parts 1.1.1 and 1.2.1, we can describe an athermal system of particles with the variables $\delta\phi = \phi - \phi_J$ and $\dot{\gamma}$. We will always assume that our system is in the thermodynamic limit $N \to +\infty \Leftrightarrow 1/L \to 0$, where L is the characteristic length and then neglect any finite-size effect arising from the finite number of particles N composing the system.

Renormalisation group theory suggests that close to the jamming point, *i.e.* $(\delta\phi \to 0, \dot{\gamma} \to 0)$, there exists $y_{\delta\phi}$ and $y_{\dot{\gamma}}$ such that the correlation length transforms under a change of length scale with a factor l as

$$\xi(\delta\phi, \dot{\gamma}) = l\xi(\delta\phi l^{y_{\delta\phi}}, \dot{\gamma} l^{y_{\dot{\gamma}}})$$

which, when choosing l such that $\delta\phi l^{y_{\delta\phi}} = -b \Leftrightarrow l = \left(-\frac{\delta\phi}{b}\right)^{-1/y_{\delta\phi}} \geq 1$, gives

$$\xi(\delta\phi, \dot{\gamma}) = \left(-\frac{\delta\phi}{b}\right)^{-1/y_{\delta\phi}} \xi\left(-b, \dot{\gamma}\left(-\frac{\delta\phi}{b}\right)^{-y_{\dot{\gamma}}/y_{\delta\phi}}\right) \underset{\delta\phi \to 0}{\sim} (-\delta\phi)^{-1/y_{\delta\phi}}$$

where we recognise $\nu = 1/y_{\delta\phi} > 0$ according to equation 1.1.

We will assume that variables which vanish at jamming are somehow linked to the free energy density of the system. Therefore, in accordance with renormalisation group theory, we here suggest the following assumption on the scaling of a vanishing variable $\mathcal{O}$ close to the jamming point for a change of length scale with a factor l

$$\mathcal{O}(\delta\phi, \dot{\gamma}) \sim l^{-y_{\mathcal{O}}/\nu} g_{\mathcal{O}}(\delta\phi l^{1/\nu}, \dot{\gamma} l^z) \tag{1.11}$$

where we can choose $\delta\phi l^{1/\nu} = -b \Leftrightarrow l = \left(-\frac{\delta\phi}{b}\right)^{-\nu} \geq 1$ and deduce

$$p(\delta\phi, \dot{\gamma}) \sim \left(\frac{\delta\phi}{b}\right)^{y_{\mathcal{O}}} g_{\mathcal{O}}\left(-b, \dot{\gamma}\left(\frac{\delta\phi}{b}\right)^{-\nu z}\right)$$

where we take the $\delta\phi \to 0$ limit, which gives

$$\mathcal{O}(\delta\phi, \dot{\gamma}) \underset{\delta\phi\to 0}{\sim} (-\delta\phi)^{y_{\mathcal{O}}} \tag{1.12}$$

with $y_{\mathcal{O}} > 0$ thus being the critical exponent associated to the vanishing of the variable $\mathcal{O}$ at jamming.

1.3.1.2 Pressure

We introduce the function $\tilde{g}_p$ such that equation 1.11 applied to the pressure p can be written

$$p(\delta\phi, \dot{\gamma}) \sim \dot{\gamma} l^z l^{-y_p/\nu} \tilde{g}_p(\delta\phi l^{1/\nu}, \dot{\gamma} l^z)$$

and then choose l such that $\delta\phi l^{1/\nu} = -b \Leftrightarrow l = \left(-\frac{\delta\phi}{b}\right)^{-\nu} \geq 1$, which leads to

$$p(\delta\phi, \dot{\gamma}) \sim \dot{\gamma}\left(-\frac{\delta\phi}{b}\right)^{-(\nu z - y)} \tilde{g}_p\left(-b, \dot{\gamma}\left(-\frac{\delta\phi}{b}\right)^{-\nu z}\right)$$

and therefore

$$\eta_p(\delta\phi, \dot{\gamma}) \equiv p(\delta\phi, \dot{\gamma})/\dot{\gamma} \underset{\delta\phi\to 0}{\sim} (-\delta\phi)^{-(\nu z - y)} \tag{1.13}$$

where we recognise $\beta = \nu z - y$ according to equation 1.1.

We now choose l such that $\dot{\gamma} l^z = b \Leftrightarrow l = \left(\frac{\dot{\gamma}}{b}\right)^{-1/z} \geq 1$, which put in equation 1.11 for p leads to

$$p(\delta\phi, \dot{\gamma}) \sim \dot{\gamma}^{y_p/\nu z} g_p\left(\delta\phi\left(\frac{\dot{\gamma}}{b}\right)^{-1/\nu z}, b\right)$$

and finally introduce the function $g_p^{(\mathrm{fit})}$ in order to ignore the constant b in this last equation, which becomes

$$p(\delta\phi, \dot{\gamma}) \sim \dot{\gamma}^{y_p/\nu z} g_p^{(\mathrm{fit})}(\delta\phi\dot{\gamma}^{-1/\nu z}) \tag{1.14}$$

and in which we will denote $q_p \equiv y_p/\nu z$ and $h_p \equiv -1/\nu z$, thus leading to $\beta = (q_p - 1)/h_p$, in addition to $Y_p \equiv p(\delta\phi, \dot{\gamma})\dot{\gamma}^{-q_p}$ and $X_p \equiv \delta\phi\dot{\gamma}^{h_p}$.

A graphical method to determine the values of ϕ_J and q_p, based on the study of equation 1.14, is described in [19], we will however use a different method that allows us to determine these parameters and h_p, and therefore find the critical exponent β.

1.3.2 Method

1.3.2.1 Fitting

Equation 1.14 suggest that it is possible to collapse the data from simulations at different packing fractions and shear strain rates on a single curve in the (X_p,Y_p) plane. To perform this fitting, we choose arbitrarily the expression of $g_p^{(\mathrm{fit})}$

$$g_p^{(\mathrm{fit})} : X_p \mapsto \exp\left(\sum_{i=0}^{5} a_{p,i} X_p^i\right)$$

and use the Levenberg-Marquardt algorithm [31, 32] with ϕ_J, q_p, h_p and $a_{p,0}$ through $a_{p,5}$ as free parameters. The goal of this algorithm is to minimise the deviation of the experimental data from the fitted curve with respect to the standard deviation for each experimental point. This is equivalent to the minimisation of the chi-square function, introduced in equation 1.16.

This then allows us to determine the relevant critical parameters at the jamming transition.

1.3.2.2 Evaluation of errors

Measurements

Variables can be measured for each choice of external parameters by averaging their values over the configurations of the system during a single shearing simulation. However, for a given variable x, we have that its values are not exactly independent from configuration to configuration.

Therefore one has to separate the different configurations of the system into blocks to which are associated an unique value of the variable x denoted X_j, indexed over th blocks of configurations. We can then calculate the standard deviation σ_x of the variable x with

$$\sigma_x^2 = \sum_{j=1}^{N_b} \frac{\langle X_j^2 \rangle - \langle X_j \rangle^2}{N_b - 1} \tag{1.15}$$

where N_b is the number of blocks, determined empirically according to the shear rate.

Fitting parameters

Errors on the parameters returned by the Levenberg-Marquardt algorithm are determined by observing how these parameters vary when including noise in the input parameters.

Quality of the fitting

Consider n experimental points (x_i, y_i), each associated with a standard deviation σ_i, which we fit with a function $y(x, a_1, \ldots, a_m)$ where $p_1, \ldots, p_m$ are free parameters. We define the *chi-square* function

$$\chi^2 \equiv \sum_{i=1}^{n} \left(\frac{y_i - y(x_i, a_1, \ldots, a_m)}{\sigma_i} \right)^2 \tag{1.16}$$

whose value should ideally be close to the number of degrees of freedom $n - m$ [33].

1.3.3 Complement on soft- to hard-core mapping

We can make use of our scaling assumption for the pressure to determine the coefficient y_E in equation 1.10.

We can fist notice that in our model of harmonic elastic interactions, the pressure and the energy scale as $E \sim p^2$ as it has already been pointed out in part 1.1.3. Therefore, we have that y_E satifies the following relation

$$y_E = 2y_p \Leftrightarrow y_E = -2q_p/h_p \tag{1.17}$$

where q_p and h_p are the exponents introduced in equation 1.14.

Therefore, considering that q_p and h_p have been determined, c remains the only unknown variable in equation 1.10. We then have a quick way to check the efficiency of this method.

Equations 1.6 and 1.10 can be rewritten as

$$\eta_p^s(\phi, \dot{\gamma}) = A \left(\phi_J - \phi + cE(\phi, \dot{\gamma})^{-h_p/2q_p} \right)^{-\beta} \tag{1.18}$$

where A is an additional parameter which can be determined if we take two points $\eta_{p,1} \equiv \eta_p(\phi_1, \dot{\gamma}_1)$ and $\eta_{p,2} \equiv \eta_p(\phi_2, \dot{\gamma}_2)$, whose corresponding energies are $E_1 \equiv E(\phi_1, \dot{\gamma}_1)$ and $E_2 \equiv E(\phi_2, \dot{\gamma}_2)$, which we hypothesise satisfy equation 1.18.

We can isolate c in equation 1.18, giving

$$c = E(\phi, \dot{\gamma})^{h_p/2q_p} \left(A^{1/\beta} \eta_p(\phi, \dot{\gamma})^{-1/\beta} - \phi_J + \phi \right)$$

which has to be satisfied by the two aforementioned points, therefore

$$E_1^{h_p/2q_p}\left(A^{1/\beta}\eta_{p,1}^{-1/\beta}-\phi_J+\phi_1\right)=E_2^{h_p/2q_p}\left(A^{1/\beta}\eta_{p,2}^{-1/\beta}-\phi_J+\phi_2\right)$$
$$\Leftrightarrow A=\left(\left(\eta_{p,1}^{-1/\beta}E_1^{h_p/2q_p}-\eta_{p,2}^{-1/\beta}E_2^{h_p/2q_p}\right)^{-1}\left(E_1^{h_p/2q_p}(\phi_J-\phi_1)+E_2^{h_p/2q_p}(\phi_2-\phi_J)\right)\right)^{\beta}$$

which can be re-injected in the expression of c evaluated in either point.

We can thus graphically evaluate the efficiency of the mapping in a log-log plot of $\eta_p(\phi,\dot{\gamma})$ versus $\phi_J-\phi_{\text{eff}}$.

Another, more time-consuming, solution is of course to apply the Levenberg-Marquardt algorithm (part 1.3.2) on equation 1.18 with A and c as free parameters.

1.4 Model of frictionless soft-core particles

1.4.1 Interactions between spherical particles

Much work on jamming has focused on a model of athermal, frictionless – *i.e.*, with no inter-particle Coulombic friction – and spherical soft-core particles with repulsive contact interaction proposed by D. J. Durian to describe foam mechanics [34], in which the rotational motion of the particles does not play any role. For two spheres $\mathcal{S}_i$ and $\mathcal{S}_j$, this model gives the following elastic potential of interaction

$$\mathcal{V}_{ij}(r_{ij})=\begin{cases}\frac{1}{2}k_e(1-r_{ij}/d_{ij})^2 & \text{if } r_{ij}\leq d_{ij}\Leftrightarrow \mathcal{S}_i\cap\mathcal{S}_j\neq\emptyset\\ 0 & \text{if } r_{ij}>d_{ij}\Leftrightarrow \mathcal{S}_i\cap\mathcal{S}_j=\emptyset\end{cases}\tag{1.19}$$

where $\vec{r_{i/j}}$ and $R_{i/j}$ are the positions and the radii of $\mathcal{S}_i$ and $\mathcal{S}_j$, $r_{ij}=||\vec{r_i}-\vec{r_j}||$ and $d_{ij}=R_i+R_j$.

This potential of interaction thus leads to the following force exterted on $\mathcal{S}_i$ by $\mathcal{S}_j$

$$\vec{f}_i^{\text{el}}(r_{ij})=\begin{cases}-\frac{k_e}{d_{ij}}(1-r_{ij}/d_{ij})\ \hat{r_{ij}} & \text{if } \mathcal{S}_i\cap\mathcal{S}_j\neq\emptyset\\ 0 & \text{if } \mathcal{S}_i\cap\mathcal{S}_j=\emptyset\end{cases}\tag{1.20}$$

where $\hat{r_{ij}}=(\vec{r_i}-\vec{r_j})/||\vec{r_i}-\vec{r_j}||$.

The original idea of Durian was to model the interaction between two bubbles in contact by the compression of two springs in series which constants would scale with the Laplace pressures, *i.e.* inversely proportionnal to the bubbles' radii, hence the harmonic potential.

Because of the finite range of the interactions, the potential energies vanish at a fixed finite radius, therefore this system is a good starting point to study macroscopic granular or colloidal systems, suspensions, foams, emulsions and liquids [8, 35].

When simulating the shearing dynamics of such a system, one has to introduce a way to dissipate the energy. This can be done with either one of these two manners, also proposed by Durian [34, 35] :

- A contact dissipation (CD) which is a pairwise interaction, additive and proportional to the difference of the velocities of the moving particles in contact,

$$\vec{f}_{\text{CD},i}^{\text{dis}}=-k_d\sum_{j\ \text{neighbours}}(\vec{v_i}-\vec{v_j})\tag{1.21}$$

  where $\vec{v_i}$ denotes the velocity of the particle i. This was originally meant to model the dissipation in the liquid between moving bubbles.

- A reservoir dissipation (RD), which is a mean-field approximation of CD where the pairwise difference of the velocities is replaced for each particle by a dissipation with respect to the average shear flow of the background reservoir,

$$\vec{f}_{\text{RD},i}^{\text{dis}}=-k_d\,(\vec{v_i}-\dot{\gamma}y_i\vec{e_x})\tag{1.22}$$

  where $\vec{v_i}$ and y_i denote the velocity and ordinate of the particle i, and $\dot{\gamma}$ and $\vec{e_x}$ denote the shearing strain rate and direction.

Therefore the translational motion of the particles is described by

$$m_i \dot{\vec{v_i}} = \vec{f_i}^{\text{el}} + \vec{f_i}^{\text{dis}} \tag{1.23}$$

To neglect the effects of inertia, we have to consider the overdamped limit $m_i \to 0$, which is easily done in the RD model. For the CD model, it is numerically necessary to take a finite value of the mass, therefore the overdamped limit has to be verified *a posteriori* [35]. However, it has been verified for sheared disks that the effect of finite mass were negligible in the CD model for shear rates $\dot{\gamma} \leq 10^{-3}$ [36].

1.4.2 Elastic force between ellipsoids

1.4.2.1 Reformulation of the elastic potential of interaction for spheres

The distance between the centres of two ellipsoids is not directly relevant to the intensity of their interactions. We need to reformulate equation 1.19 with parameters which would be relevant for ellipsoids. In [37], the overlap potential of two ellipsoids is a function of μ the rescaling factor by which the particles need to be resized in order to be externally tangent.

Consider two spheres $\mathcal{S}_i$ and $\mathcal{S}_j$, we will denote $\forall \vec{r} \in \mathbb{R}^3$, $\mu_i(\vec{r})$ and $\mu_j(\vec{r})$ the rescaling factor that has to be applied to $\mathcal{S}_i$ and $\mathcal{S}_j$ respectively for $\vec{r}$ to be on their surface.

We can show there exists a point $\vec{r_C}$ on the segment connecting their centres for which $\mu_i(\vec{r_C}) = \mu_j(\vec{r_C}) = \mu(\vec{r_i}, \vec{r_j}) = r_{ij}/d_{ij}$, where $\mu(\vec{r_i}, \vec{r_j})$ is the rescaling factor for which both spheres are externally tangent. Therefore, we can reformulate equation 1.19

$$\mathcal{V}_{ij}(\vec{r_i}, \vec{r_j}) = \begin{cases} \frac{1}{2} k_e (1 - \mu(\vec{r_i}, \vec{r_j}))^2 & \text{if } \mathcal{S}_i \cap \mathcal{S}_j \neq \emptyset \\ 0 & \text{if } \mathcal{S}_i \cap \mathcal{S}_j = \emptyset \end{cases} \tag{1.24}$$

1.4.2.2 Elastic force between ellipsoids

We will assume that equation 1.24 remains valid for two ellipsoids $\mathcal{A}$ and $\mathcal{B}$ of respective centres $\vec{r}_{\mathcal{A}}$ and $\vec{r}_{\mathcal{B}}$,

$$\mathcal{V}_{\mathcal{AB}}(\vec{r_{\mathcal{A}}}, \vec{r_{\mathcal{B}}}) = \begin{cases} \frac{1}{2} k_e (1 - \mu(\vec{r_{\mathcal{A}}}, \vec{r_{\mathcal{B}}}))^2 & \text{if } \mathcal{A} \cap \mathcal{B} \neq \emptyset \\ 0 & \text{if } \mathcal{A} \cap \mathcal{B} = \emptyset \end{cases} \tag{1.25}$$

where $\mu(\vec{r}_{\mathcal{A}}, \vec{r}_{\mathcal{B}})$ is the rescaling factor that has to be applied to $\mathcal{A}$ and $\mathcal{B}$ for them to be externally tangent.

Therefore, the force exerted on $\mathcal{A}$ by $\mathcal{B}$ is

$$\begin{aligned} \vec{f}^{\text{el}}_{\mathcal{AB}}(\vec{r_{\mathcal{A}}}, \vec{r_{\mathcal{B}}}) &= -\frac{d\mathcal{V}_{\mathcal{AB}}}{d\vec{r_{\mathcal{A}}}}(\vec{r_{\mathcal{A}}}, \vec{r_{\mathcal{B}}}) \\ &= k_e (1 - \mu(\vec{r_{\mathcal{A}}}, \vec{r_{\mathcal{B}}})) \frac{d\mu}{d\vec{r_{\mathcal{A}}}}(\vec{r_{\mathcal{A}}}, \vec{r_{\mathcal{B}}}) \end{aligned} \tag{1.26}$$

Please refer to appendix A for an explicit expression of this force.

1.4.3 Dissipative force between ellipsoids

The expressions proposed for the dissipative force exerted on a particle i by a particle j in equations 1.21 and 1.22 remain relevant for ellipsoids.

However, we now have that the elastic force exerted by an ellipsoid on another can induce a rotational motion of both particles. Authors of [38] had already proposed for spheres to couple rotational and translational motion by taking into account the rotation velocities of the particles in the contact dissipation model of the dissipative force

$$\vec{f}_{ij}^{\text{dis}} = -k_d (\vec{v_i}^{C_j} - \vec{v_j}^{C_i}) \tag{1.27}$$

where $\vec{v_i}^{C_j}$ is the local velocity of particle i at its point of contact $\vec{r}_{C,i}$ with particle j.

Consider two ellipsoids $\mathcal{A}$ and $\mathcal{B}$, whose centres are located in $\vec{r_{\mathcal{A}}}$ and $\vec{r_{\mathcal{B}}}$, whose velocities are $\vec{v_{\mathcal{A}}}$ and $\vec{v_{\mathcal{B}}}$. Then, we can calculate the local velocity of the ellipsoids at their points of contact

$$\begin{aligned} \vec{v_{\mathcal{A}}}^{C_{\mathcal{A}}} &= \vec{v_{\mathcal{A}}} + \vec{\omega_{\mathcal{A}}} \times (\vec{r_{C,\mathcal{A}}} - \vec{r_{\mathcal{A}}}) \\ \vec{v_{\mathcal{B}}}^{C_{\mathcal{B}}} &= \vec{v_{\mathcal{B}}} + \vec{\omega_{\mathcal{B}}} \times (\vec{r_{C,\mathcal{B}}} - \vec{r_{\mathcal{B}}}) \end{aligned} \tag{1.28}$$

where $\vec{\omega_i}$ is the rotation vector of i.

1.4.4 Pressure in a sheared packing of ellipsoids

To determine the pressure in the system, we have to determine its pressure tensor P which is made of three parts [38, 39]

(i) the kinetic part

$$P_{\text{kin}} = \frac{1}{L^2} \sum_{i<j} m_i \vec{\delta v_i} \vec{\delta v_i}^T \tag{1.29}$$

with m_i the mass of particle i and $\vec{\delta v_i}$ the fluctuation of the velocity of particl i away from the average velocity profile which caracterises the flow,

(ii) the dissipative part

$$P_{\text{dis}} = \frac{1}{L^2} \sum_{i<j} \left(\vec{f}_{ij}^{\text{dis}} \left(\vec{r_{C,i}} - \vec{r_i}\right)^T + \vec{f}_{ji}^{\text{dis}} \left(\vec{r_{C,j}} - \vec{r_j}\right)^T \right) \tag{1.30}$$

with $\vec{f}_{ij}^{\text{dis}}$ the dissipative force exerted on particle i by particle j (equation 1.27), $\vec{r_{C,i}}$ the point of contact on particle i and $\vec{r_i}$ the centre of particle i,

(iii) and the elastic part [39]

$$P_{\text{el}} = \frac{1}{L^2} \sum_{i<j} \left(\vec{f}_{ij}^{\text{el}} \left(\vec{r_{C,i}} - \vec{r_i}\right)^T + \vec{f}_{ji}^{\text{el}} \left(\vec{r_{C,j}} - \vec{r_j}\right)^T \right) \tag{1.31}$$

with $\vec{f}_{ij}^{\text{dis}}$ the dissipative force exerted on particle i by particle j (equation 1.26), leading to

$$P = P_{\text{kin}} + P_{\text{dis}} + P_{\text{el}} \tag{1.32}$$

from which we define the average pressure of the system as

$$p = \frac{1}{D} \text{Tr}(P) \tag{1.33}$$

where $D = 3$ is the dimension of the system.

Most often in shearing simulations, for small enough shear strain rates $\dot{\gamma}$, the elastic part of the pressure

$$p_{\text{el}} = \frac{1}{D} \text{Tr}(P_{\text{el}}) \tag{1.34}$$

dominates over the kinetic and dissipative parts [40]. We will then identify the pressure and its elastic part without further notice.

1.4.5 Dispersity

As we have pointed out in part 1.2.1, polydispersity is necessary to prevent crystallisation. In our simulations we use two sizes of ellipsoids in equal number, with a corresponding axis ratio of 1.4 between these sizes. We chose the masses of the ellipsoids to be $m = 1$ and $m = 1.4^3$ to ensure that ellipsoids of both sizes have the same density.

1.5 Rheology

The shearing rheology of athermal frictionless soft-core disks has been thoroughly studied in [38, 40] and gives hints on what to expect of the shearing rheology of spheroids in our model near the jamming transition. Authors of these papers stressed that the model chosen for the dissipation was determinant to the behaviours observed. In this part we will only focus on the contact dissipation model which takes into account the rotation of the particles (equation 1.27).

Vågberg *et al.* showed that upon increasing the packing fraction, disks sharply transitioned from Bagnoldian rheology

$$\sigma, p \sim \dot{\gamma}^2 \Leftrightarrow \frac{\partial}{\partial \dot{\gamma}} B_{\sigma,p} = 0,\ B_{\sigma,p} \equiv \sigma, p/\dot{\gamma}^2 \tag{1.35}$$

to Newtonian rheology

$$\sigma, p \sim \dot{\gamma} \Leftrightarrow \frac{\partial}{\partial \dot{\gamma}^2} \eta_{\sigma,p} = 0,\ \eta_{\sigma,p} \equiv \sigma, p/\dot{\gamma} \tag{1.36}$$

at a precise packing fraction which depended on the inelasticity of collisions between particles, as measured by the parameter $Q \propto \sqrt{mk_e/k_d^2}$ with m, k_e and k_d introduced in equations 1.19, 1.21 and 1.22.

We will call $B_{\sigma,p}$ the *Bagnoldian transport coefficient* associated to shear strain or pressure and $\eta_{\sigma,p}$ the *Newtonian transport coefficient* associated to shear strain or pressure.

At low packing fractions, *i.e.* for dilute systems, particles separate if the contact velocity is not damped to zero during the collision, which is possible for elastic enough interactions. Particles in such systems have few instantaneous contacts; In this case, the system is in an "inertial" regime: the dissipation term in equation 1.23 is negligible and the trajectories are determined by the balance of elastic and kinetic terms, hence the Bagnoldian rheology at small $\dot{\gamma}$ [40]. Shearing simulations showed that disks are able to adjust their rotation to cancel out the relative motion of particles, so that the tangential component of the contact velocity difference is as small as the normal component, hence the small dissipative force [38].

At high packing fractions, *i.e.* for dense systems, compressive motion which would induce particle overlaps is energetically prohibitive. Normally directed relative motion is thus greatly suppressed and the collisions are primarily tangential. Shearing simulations have showed that, in this case, disks fluctuate in their rotational motion but that these fluctuations are uncorrelated with the tangential component of the velocity difference, thus leading to a large tangential component of the dissipative force compared to its normal component. This lack of correlations of the rotation is thought to result from the increasing constraint on rotational motion due to the higher number of contacts at higher densities [38]. The system is then in an "overdamped" regime: the kinetic term in equation 1.23 is negligible and the trajectories are determined by the balance of elastic and dissipative terms, hence the Newtonian rheology at small $\dot{\gamma}$ [40]. Because of the tangential dissipation, particles tend to cluster together, with force chains percolationg throughout the systems, and have more instantaneous contacts.

Furthermore, authors showed that η_p was independent of Q in the Newtonian regime and that their system was always Newtonian at jamming. Therefore, they concluded that the value of ϕ_J as well as the exponent characterising the divergence of η_p should be independent of the inelasticity of collisions, *i.e.* of the parameters m, k_e and k_d [38].

2 | Results and discussion

2.1 Preliminary results

Preliminary simulations were performed with only 64 particles, first to ensure that our models and methods were effective and gave realistic results, then to determine what phenomena were different with ellipsoids than with spheres. Simulations performed with this few particles have the advantage to quickly give results to analyse, however finite-size effects are not negligible and can affect the jamming transition (see part 1.1.5).

2.1.1 Rheological transition

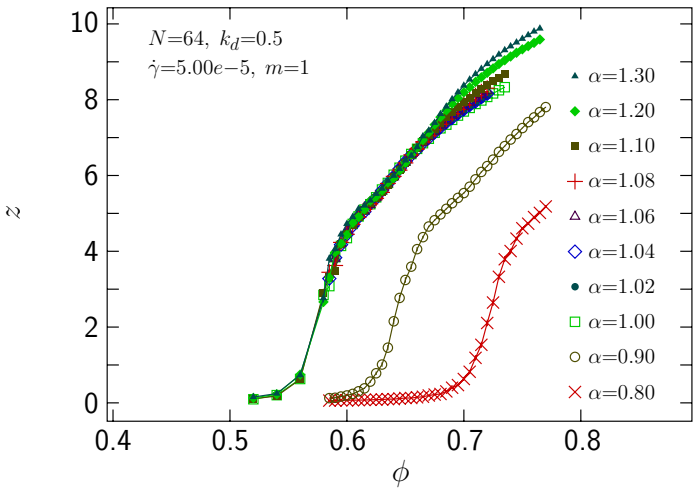

Figure 2.1: Average contact number per particle as a function of the packing fraction for aspect ratios $0.8 \leq \alpha \leq 1.3$. $N = 64,\ k_d = 0.5,\ \dot{\gamma} = 5e-5,\ m = 1$.

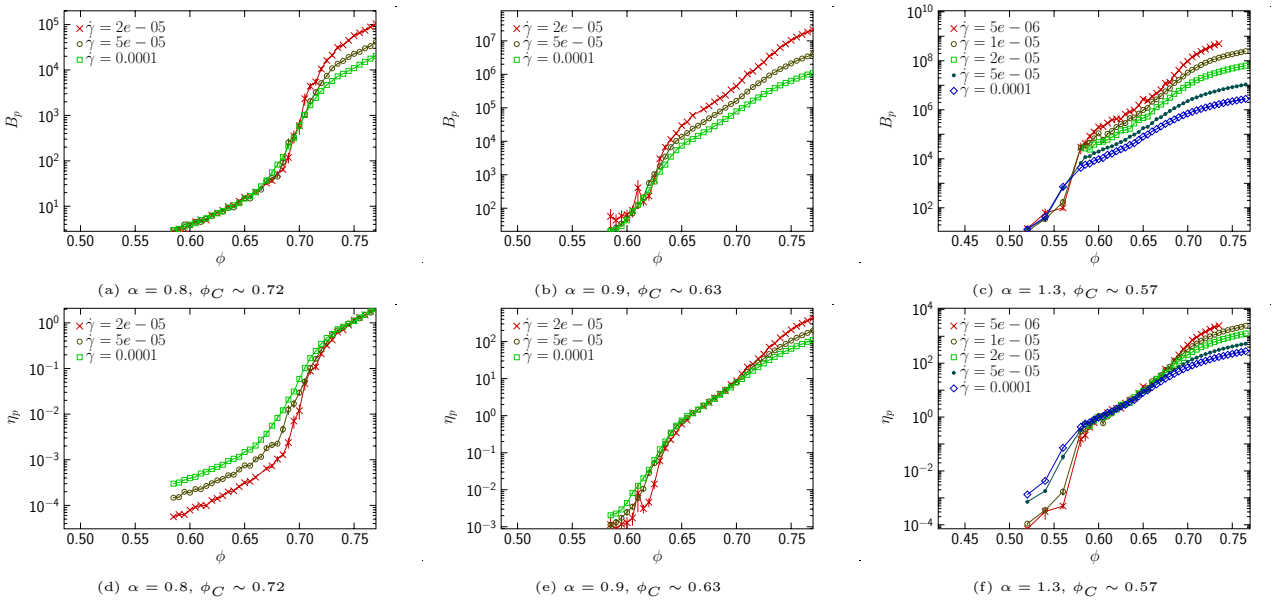

Figure 2.2: Bagnoldian (figures 2.2a, 2.2b and 2.2c) and Newtonian (figures 2.2d, 2.2e and 2.2f) transport coefficients associated to pressure. $N = 64,\ k_d = 0.5,\ m = 1$. We denote ϕ_C the transition packing fraction.

We observe in figure 2.1 a sharp increase in the average contact number per particle upon increasing the packing fraction. According to the development of part 1.5, this increase is the sign of a transition from Bagnoldian rheology to Newtonian rheology. We confirm this by determining the Bagnoldian and Newtonian transport coefficients associated to pressure as functions of the packing fraction, and verifying the transitions from a regime to the other occurs at the same packing fractions as the increase of contact number (figure 2.2).

We also observe that the Newtonian transport coefficients become $\dot{\gamma}$-dependent for high enough packing fractions, we will see in part 2.1.2.1 that this is due to a deviation from the hard-core limit near the jamming transition.

Moreover, we can notice that for $1 \leq \alpha < 1.3$ (sphere and prolate spheroids) the transition from the Bagnoldian to the Newtonian regime occurs approximately at the same packing fraction, while for $\alpha = 0.8, 0.9$ (oblate spheroids) the transition packing fraction ϕ_C varies with the aspect ratio and is higher than the value obtained for the former particles.

2.1.2 Critical behaviour

2.1.2.1 Deviation from the hard-core limit close to jamming

We expect from the development of part 1.5 that the system would display Newtonian rheology sufficiently close to the jamming transition, *i.e.* that the Newtonian transport coefficients would be independent of the shear rates at which they are determined. However, this holds only in the hard-core limit.

Close to the jamming transition, the overlapping of the particles is non-negligible, hence the deviation from the hard-core limit. This deviation being even more important for higher shear strain rates (figure 2.3).

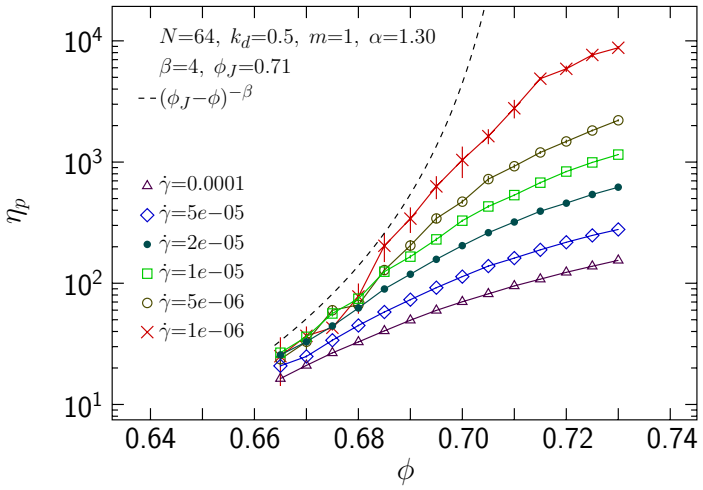

Figure 2.3: Newtonian coefficient of transport associated to pressure as a function of the packing fraction for $\alpha = 1.3$.

2.1.2.2 Effectiveness of scaling

Figure 2.4a shows that we have successfully made experimental data from simulations at different density and shear strain rates collapse on a single curve with the method described in part 1.3, thus confirming its effectiveness. From the scaling exponents of this graph, we made collapse on a single straight line the Newtonian transport coefficients associated to pressure inferred from simulations at different shear rates. This straight line characterises the critical behaviour described by equation 1.1 for hard-core particles. This collapsing shows satisfactory visual precision in figure 2.4b.

Moreover, we can notice that the mapping parameters determined graphically in figure 2.4b ($A = 1.9$, $c = 0.48$) are close to the values found in [20] for disks ($A = 1.53$, $c = 0.458$).

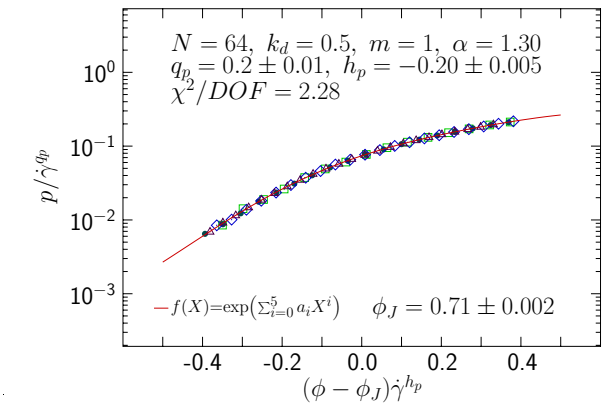

(a) Pressure scaling plot, as described in part 1.3.1.2.

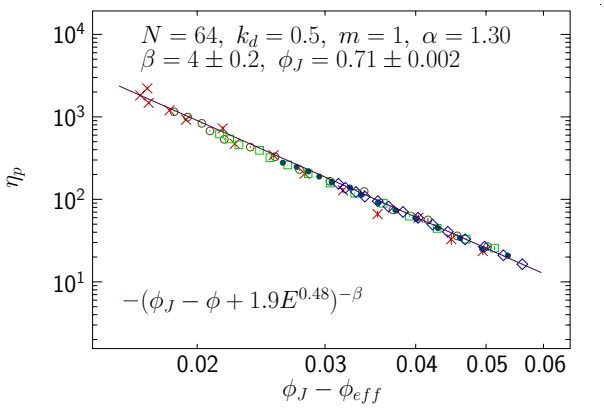

(b) Newtonian transport coefficient associated to pressure scaling plot, obtained with the soft- to hard-core mapping method described in parts 1.2.3 and 1.3.3. We privileged here the graphical determination of the mapping parameters.

Figure 2.4: Scaling plots for $\alpha = 1.3$.

2.1.2.3 Jamming density and critical exponent

From plots such as figure 2.4a we were able to determine the jamming density and critical exponents for different aspect ratios (see figure 2.5).

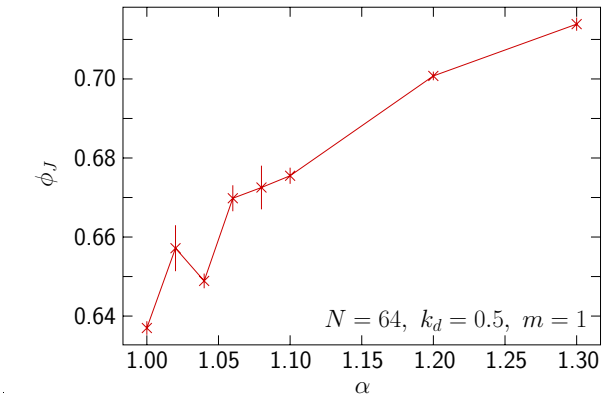

(a) Jamming packing fraction as a function of the aspect ratio.

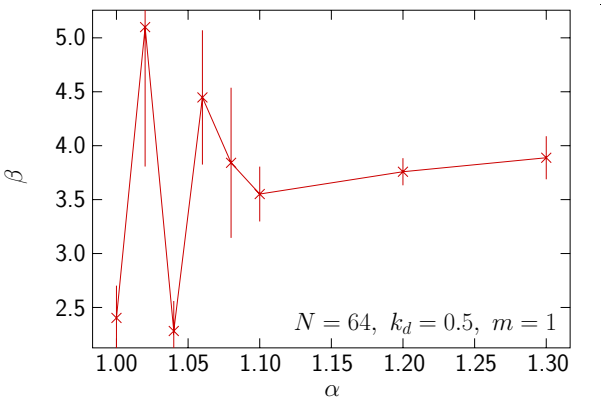

(b) Critical exponent associated to the divergence of the Newtonian transport coefficients as a function of the aspect ratio.

Figure 2.5: Jamming parameters for spheres and prolate spheroids.

We can first notice that for $\alpha = 1$, *i.e.* for spheres, we have $\beta \sim 2.5$ which is close to the result of [20] for disks ($\beta = 2.58$). Moreover, we have the jamming packing fraction $\phi_J \sim 0.64$ close to the random close packing fraction for spheres [25].

For the set of aspect ratios considered ($1 \leq \alpha \leq 1.3$), we have that the jamming packing fraction is an increasing function of the aspect ratio (figure 2.5a) – if we exclude $\alpha = 1.04$. This is in accordance with [25] which found that ϕ_J was an increasing function of the aspect ratio for $1 \leq \alpha \lesssim 1.6$. Simulations with 64 particles were performed for oblate particles but not close enough to the jamming transition to give ϕ_J and β with good precision. Nonetheless, we also observed for these particles that the jamming packing fraction would be greater than its value for packings of spheres. More specifically, we estimated $0.7 < \phi_J(\alpha = 0.9) < \phi_J(\alpha = 0.8)$.

It is more difficult to predict the behaviour of the critical exponent β from figure 2.5b. However – if we exclude $\alpha = 1.04$ once again – we can assume that the critical exponent associated to the divergence of the Newtonian transport coefficients is higher for prolate spheroids than for spheres and has a value close to ~ 4.

2.1.3 Orientation

Following the claim that shearing breaks the isotropy of space in part 1.1.4, we wished to check if

(i) spheroids tend to angle themselves in a particular direction,

(ii) the orientation of the spheroids is correlated.

2.1.3.1 Direction of orientation

We denote O_i the mean over configurations of the system of the square of the projection of the axis of symmetry of the spheroid on the i^{th} axis, with then $\sum_{i=1}^{3} O_i^2 = 1$ and the 0^{th} and 1^{st} axis corresponding the directions of the shear and the gradient of shear velocity respectively.

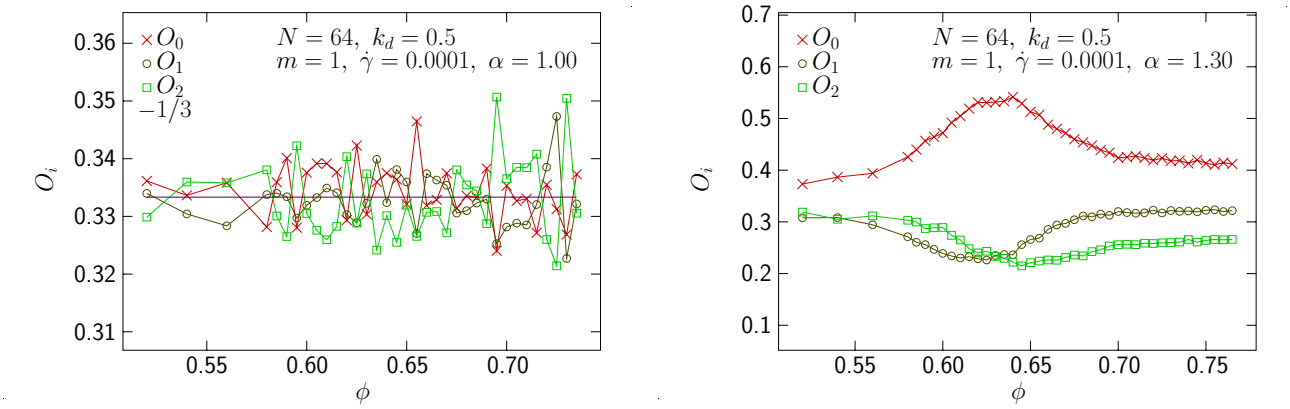

(a) $\alpha = 1$. Straight line corresponds to $O_i = 1/3$.

(b) $\alpha = 1.3$

Figure 2.6: Mean squared orientation of the axis of symmetry of the particles.

We expect that all orientations are equivalent for spheres, which is confirmed by figure 2.6a in which the projections do not show any particular behaviours.

For spheroids we see that the 0^{th} direction may be privileged since the mean squared projection of the axis of symmetry on this direction describes a well-defined peak around a given packing fraction while the projections on the other directions reach their minimum around this same packing fraction but both at different densities though (figure 2.6b).

Moreover, since the projection curves on the 1^{st} and 2^{nd} directions are well-defined – contrarily to the curves in figure 2.6a – we cannot say that the shear direction is the only relevant direction in our system.

Prolate spheroids

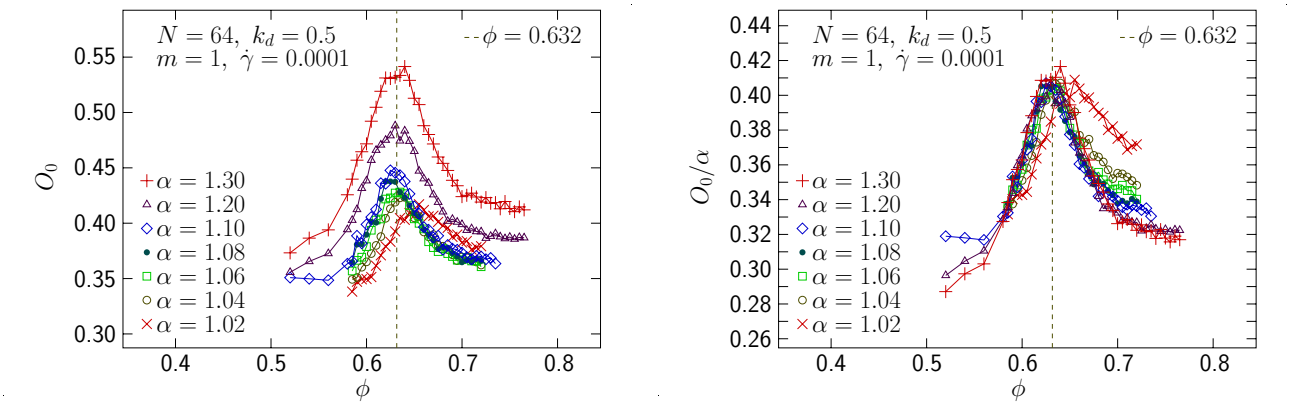

(a) Raw projections.

(b) Projections ratioed with the aspect ratio.

Figure 2.7: Mean of the squared projection of the axis of symmetry of the particles on shear direction as a function of the packing fraction.

For all the aspect ratios greater than one we have tested, the mean projection of the axis of symmetry of the particles on the shear direction reaches a well-defined peak (figure 2.7a). We have that the height of this peak is approximately proportional to the aspect ratio α (figure 2.7b).

We can notice that the packing fractions at which these peaks appear are somewhat lower than the jamming densities corresponding to the aspect ratios. Indeed, we can read $\phi_J(\alpha > 1) \gtrsim 0.65$ from figure 2.5a. They are also undoubtedly higher than the rheological transition packing fractions (figure 2.1) and therefore these peaks do not correspond to any transition or phenomenon we have already described or expected.

Furthermore, what figure 2.7b also shows is that the position of the peak is much less dependent of the aspect ratio than the jamming density, and even seems not to vary at all – if we exclude $\alpha = 1.02$. However, it should be delicate to extrapolate such a result to hard-core particles since the overlaps are not negligible this close to the jamming transition, which suggests that we should rather be attentive to these variables as functions of the effective packing fraction (figure 2.8).

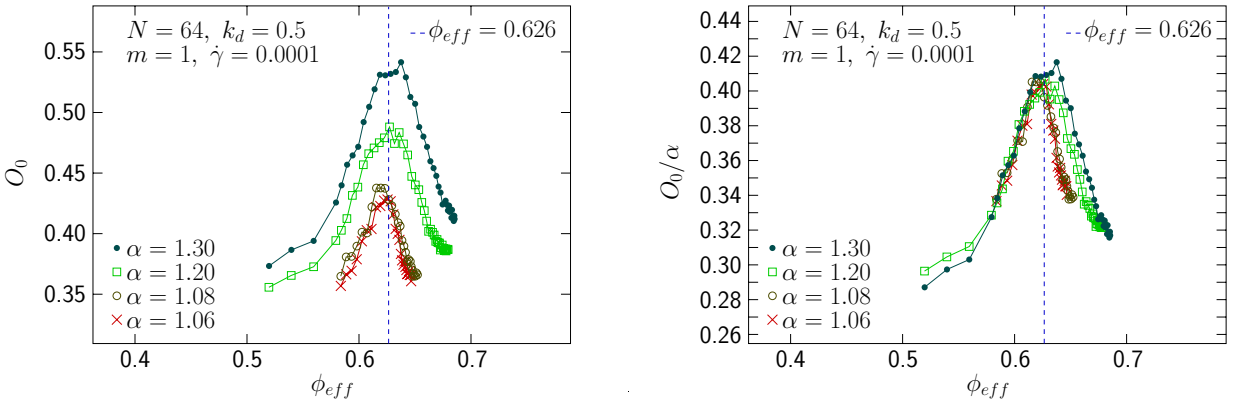

(a) Raw projections.

(b) Projections ratioed with the aspect ratio.

Figure 2.8: Mean projection of the axis of symmetry of the particles on the direction of the shear rate as a function of the effective packing fraction. We only show the aspect ratios for which the soft- to hard-core mapping gives a satisfactory visual precision.

A quick visual analysis of figure 2.8 shows that the effective packing fraction at which the projection of the axis of symmetry of prolate spheroids on the shear direction reaches its peak is also much less dependent of the aspect ratio than the jamming packing fraction is.

We can also be interested in knowing if the observations on the projection of the axis of symmetry on the shear direction (figure 2.7) hold for the two other projections (figure 2.9).

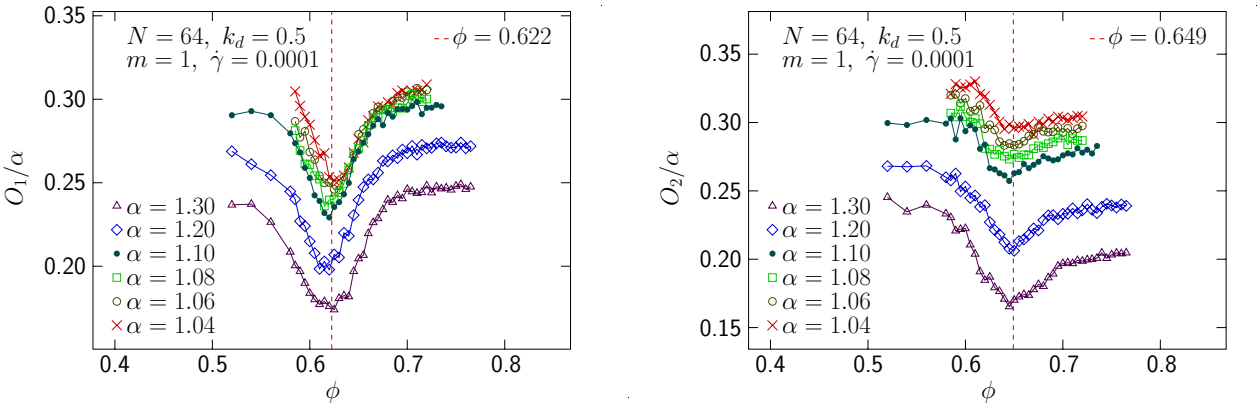

(a) Projection on the direction of the gradient of shear rate.

(b) Projection on the 2nd direction.

Figure 2.9: Mean of the squared projections of the axis of symmetry of the particles as functions of the packing fraction.

As expected from figure 2.6b, both projections reach a minimum which position, for a given aspect ratio, depends on the axis of projection. We observe that the packing fraction at which O_0 reaches its maximum (see figure 2.7) is higher than the packing fraction at which O_1 reaches its minimum and lower than than the packing fraction at which O_2 reaches its minimum, in accordance with figure 2.6b.

There is no relation of proportionality between the depths of the minimums and the aspect ratio for these projections, contrarily to what we would have expected from figure 2.7b. Moreover, we observe that for $1 < \alpha < 1.3$, *i.e.* for not too elongated prolate spheroids, the minimum reached by O_1 is lower than the minimum reached by O_2.

We still observe that the positions of the minimums are much less dependent of the aspect ratio than the jamming density, as we observed for the projection on the shear direction.

Oblate spheroids

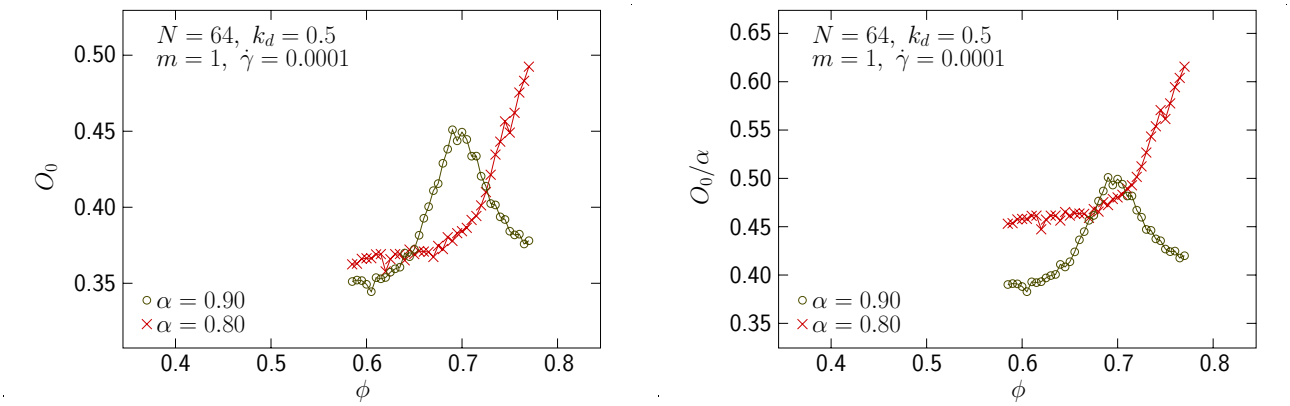

(a) Raw projections.

(b) Projections ratioed with the aspect ratio.

Figure 2.10: Mean projection of the axis of symmetry of the particles on the direction of the shear rate as a function of the packing fraction.

We do not have data at sufficiently high packing fraction to observe the peak of the projection of the axis of symmetry on the shear direction for $\alpha = 0.8$, however the data presented in figure 2.10 clearly shows that we should expect for oblate spheroids that the position of the peak strongly depends on the aspect ratio and moreover that its height is not proportional to the aspect ratio, contrarily to prolate spheroids.

This, in addition to the fact that the rheological transition also does not appear at the same packing fractions for oblate spheroids contrarily to prolate spheroids (part 2.1.1), shows that the behaviour of packings of prolate and oblate spheroids is very different, and suggest we may expect the mechanisms governing the jamming transition for these types of particles to be different.

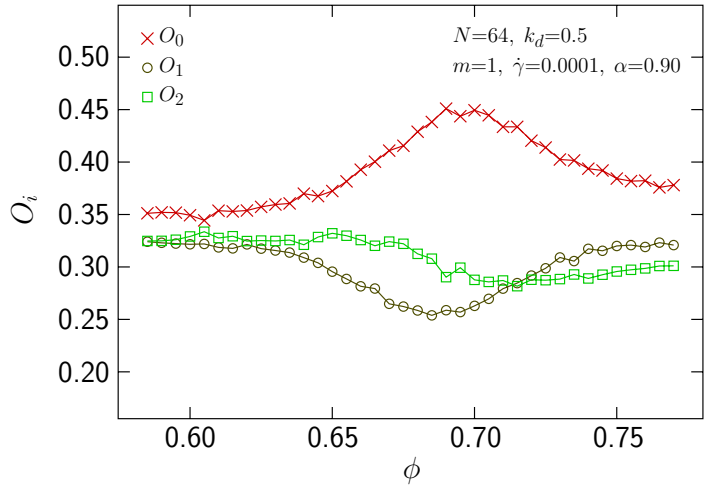

Figure 2.11: Mean squared orientation of the axis of symmetry of the particles for $\alpha = 0.8$.

Otherwise, we expect the observations we have made about the projections on all axis as functions of the packing fraction for a given aspect ration (see figure 2.6b) to remain valid for oblate spheroids (see figure 2.11).

2.1.3.2 Correlation

$\mathcal{C}_{ij}$ is a function which increases with increasing correlation between the orientations of the spheroids.

Prolate spheroids

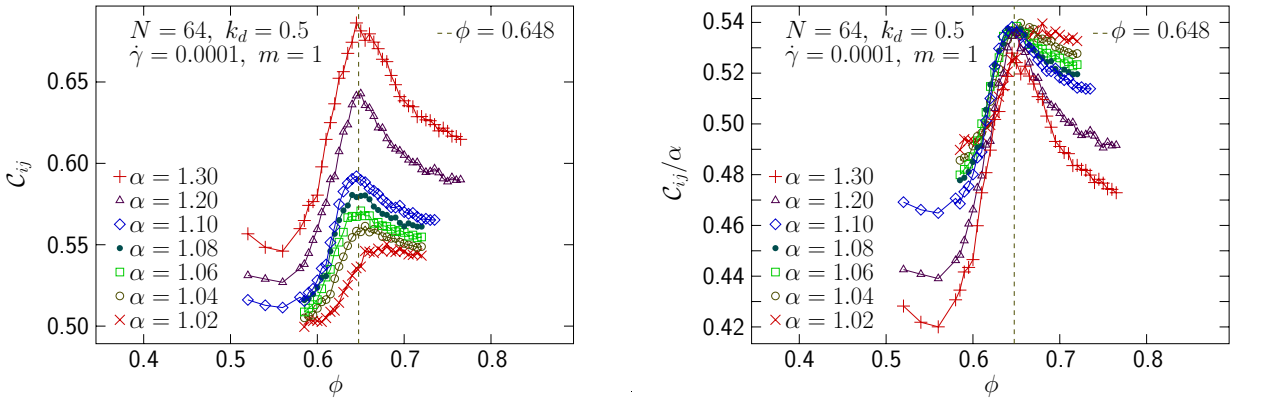

(a) Raw correlation function.

(b) Correlation function ratioed with the aspect ratio.

Figure 2.12: Orientation correlation as a function of the packing fraction.

As the mean squared projection of the axis of symmetry on the shear direction (see figure 2.7), the correlation function $\mathcal{C}_{ij}$ reaches a peak which height is proportional to the aspect ratio if we let aside $\alpha = 1.3$, *i.e.* if we only consider not too elongated prolate spheroids. Moreover, the position of this peak is much less dependent of the aspect ratio than the jamming density (see figure 2.12).

However, despite the striking resemblance of the aforementioned figures, we have that $\mathcal{C}_{ij}$ reaches its maximum at a packing fraction slightly higher than the packing fraction at which O_0 reaches its. Indeed, it rather seems to correspond to the packing fraction at which O_2 reaches its minimum (see figure 2.9b).

Oblate spheroids

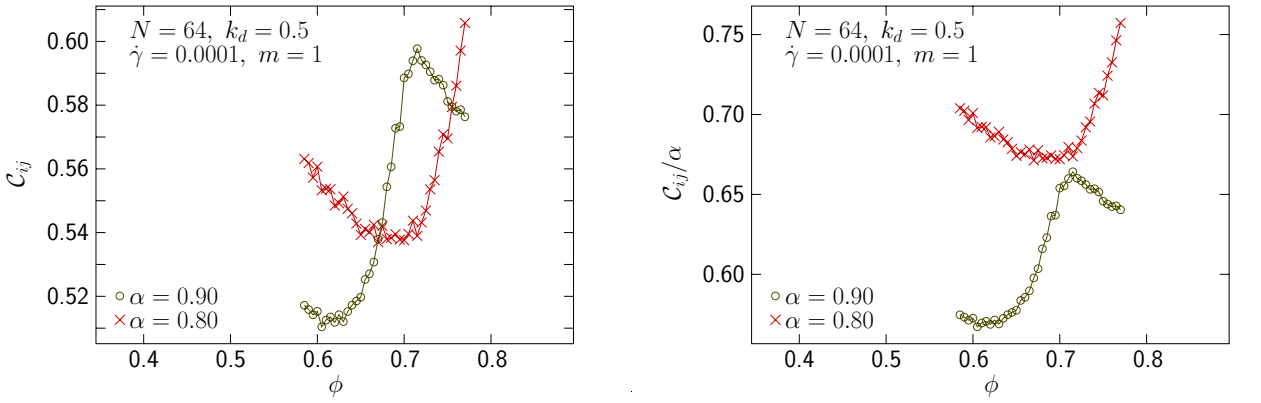

(a) Raw correlation function.

(b) Correlation function ratioed with the aspect ratio.

Figure 2.13: Orientation correlation as a function of the packing fraction.

As for the projection of the axis of symmetry on the shear direction for oblate particles (see figure 2.10), we observe here that the position of the peak of correlation function strongly depends on the aspect ratio for oblate particles (see figure 2.13), contrarily to prolate particles (see figure 2.12) – even though data at higher packing fractions and for more aspect ratios would be needed.

Moreover, and still in accordance to what we have observed for the aforementioned projection, there is no relation of proportionality between the value of the maximum of the correlation function and the aspect ratio for oblate particles.

2.2 Dominance of the elastic pressure

We claimed in part 1.4.4 that the elastic part of the pressure, p_{el}, was the main contribution to the total pressure, p.

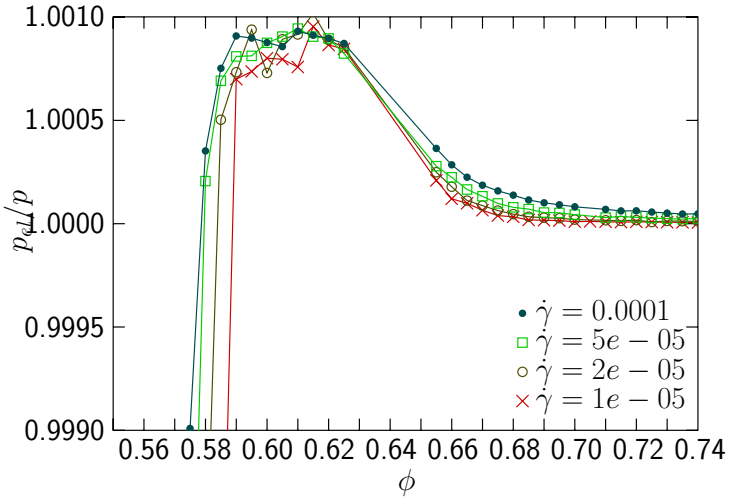

Figure 2.14: Ratio of the elastic pressure p_{el} and the total pressure p.

Figure 2.14 shows that, for $0.59 \leq \phi \leq 0.74$, approximating the total pressure by its elastic part gives an error lesser than 0.1%, thus justifying our claim. We will then use the notation p to designate p_{el}.

2.3 Relaxation time

Relaxation simulations, of which the method is described in part 1.2.2, were performed with 16384 particles.

2.3.1 Exponential decay of the pressure

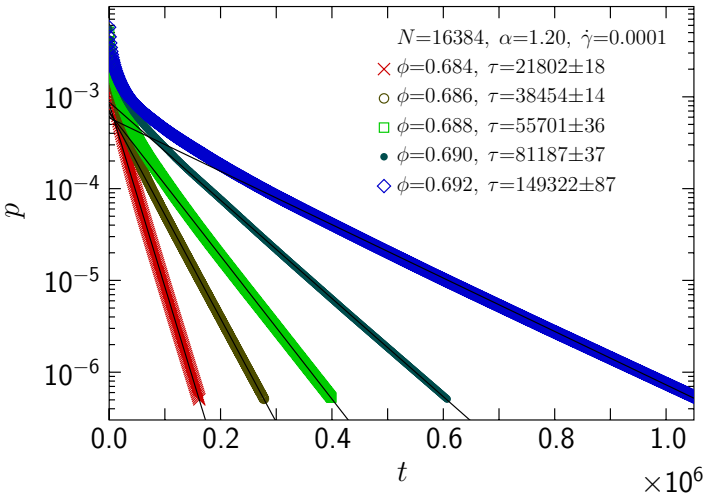

Figure 2.15: Semi-log plot of the pressure versus the time, where $t = 0$ corresponds to the time the shearing stopped.

We predicted that after a short transient time, the pressure would decay exponentially to zero with a characteristic time scale $\tau(\phi, \dot{\gamma})$ – named the relaxation time – where ϕ is the packing fraction and $\dot{\gamma}$ the shear strain rate before the relaxation phase (see part 1.1.3, and especially equation 1.2). We confirm these predictions with figure 2.15.

2.3.2 Scaling of the relaxation time with the packing fraction

Figure 2.15 indicates that the relaxation time would increase with increasing packing fractions for systems below jamming, which is what suggested by equations 1.4 and 1.5. By plotting the relaxation time versus the difference to the jamming packing fraction in a log-log plot, we should then be graphically able to determine both the critical exponent β and the jamming transition ϕ_J (see figure 2.16).

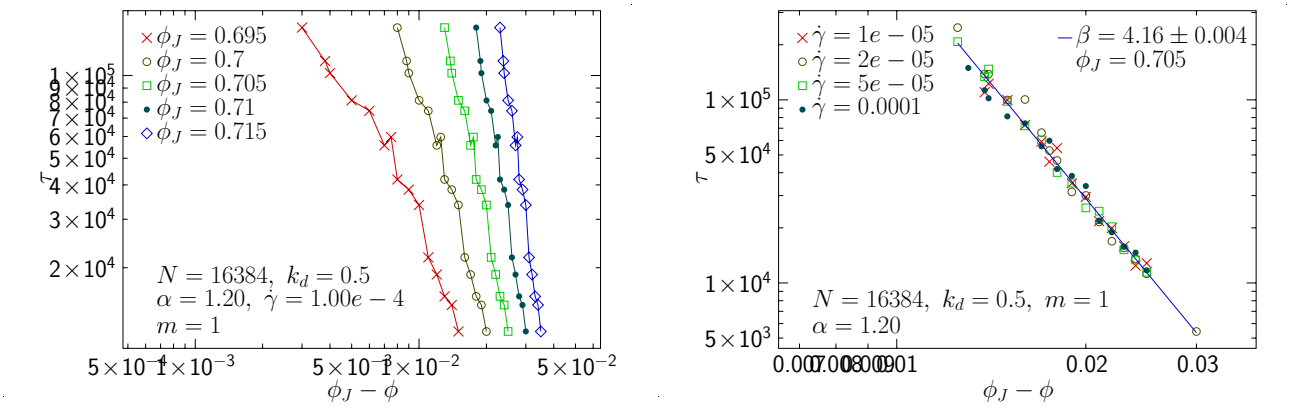

(a) Graphical determination of ϕ_J.

(b) Linear regression to determine β.

Figure 2.16: Graphical determination of the critical exponent β and the jamming packing fraction ϕ_J.

From figure 2.16a we can visually determine that the jamming packing fraction is $\phi_J \sim 0.705$. We then plot the relaxation time τ versus $\phi_J - \phi$ to determine from the slope the critical exponent $\beta \sim 4.16$. These results are consistent with those obtained from the shearing method with 64 particles (see figure 2.5).

Simulations for densities closer to the jamming packing fraction and for other aspect rations have not been performed yet, the relaxation process being too long to have precise enough data within a month. Still, figure 2.16 shows the efficiency of our method.

Conclusion

In this work, we have presented models and methods which allowed us to investigate the jamming transition of spheroidal particles through shearing simulations.

Preliminary results are in good accordance with the existing literature, which reinforces the trust in our models, and also showed new and interesting results. We found that the rheological transition always happened at the same packing fractions for prolate spheroids, while it was strongly dependent of the aspect ratio for oblate spheroids (see part 2.1.1). In addition to this, we found that spheroidal particles in a sheared packing tended to angle themselves in a particular direction and with an important correlation for a packing fraction which does not correspond to the rheological transition or the jamming transition (see part 2.1.3). This packing fraction was also independent of the aspect ratio for prolate spheroids and not for oblate spheroids.

These interesting results could give new insights into the jamming transition. Indeed, we have seen in part 1.5 that the rheology of the system and the orientations of the particles are intimately related to the way particles pack. Our results could then suggest that different mechanisms govern the jamming transition for prolate and oblate spheroids. Further studies are necessary to understand what are the causes and consequences of these phenomena.

An other relevant variable to describe the jamming transition is the mean number of contacts [8, 21, 25, 37, 41]. In particular, there have been recent claims that packings of ellipsoids would be hypostatic at jamming – *i.e.*, the total number of contacts is lesser than the total number of degrees of freedom – but it was only demonstrated for static packings. Further studies with our methods could bring an other explanation to this phenomenon.

Finally, the study of the jamming transition as a critical phenomenon raises the question of the universality of our critical exponents. We showed that for prolate particles, the critical exponent associated to the vanishing of the pressure was close to 4 for prolate spheroids while it was close to 2.5 for spheres. Further studies are necessary to determine if the value of this exponent is universal for all spheroids, and if not how it should vary and why.

References

[1] Richard Patrick, Mario Nicodemi, Renaud Delannay, Philippe Ribiere, and Daniel Bideau. Slow relaxation and compaction of granular systems. *Nature materials*, 4(2):121, 2005.

[2] National Science Foundation. Granular materials – YouTube. https://www.youtube.com/watch?v=R7g6wdmYB78. [Online; accessed 13-July-2017].

[3] Andrea J Liu and Sidney R Nagel. Nonlinear dynamics: Jamming is not just cool any more. *Nature*, 396 (6706):21–22, 1998.

[4] Peter Olsson and Stephen Teitel. Critical scaling of shear viscosity at the jamming transition. *Physical review letters*, 99(17):178001, 2007.

[5] Daniel Vågberg, Peter Olsson, and Stephen Teitel. Glassiness, rigidity, and jamming of frictionless soft core disks. *Physical Review E*, 83(3):031307, 2011.

[6] Pierre-Gilles de Gennes. Granular matter: a tentative view. *Reviews of modern physics*, 71(2):S374, 1999.

[7] Leo P Kadanoff. Built upon sand: Theoretical ideas inspired by granular flows. *Reviews of Modern Physics*, 71(1):435, 1999.

[8] Corey S O'hern, Leonardo E Silbert, Andrea J Liu, and Sidney R Nagel. Jamming at zero temperature and zero applied stress: The epitome of disorder. *Physical Review E*, 68(1):011306, 2003.

[9] Junyao Tang and R.P. Behringer. How granular materials jam in a hopper (processed) – YouTube. https://www.youtube.com/watch?v=lWSJwZhqoQw. [Online; accessed 29-June-2017].

[10] Junyao Tang. Ellptical particles flowing in a hopper – YouTube. https://www.youtube.com/watch?v=p3lwWfF2dTI. [Online; accessed 29-June-2017].

[11] Kiwing To, Pik-Yin Lai, and HK Pak. Jamming of granular flow in a two-dimensional hopper. *Physical review letters*, 86(1):71, 2001.

[12] B Eisenblätter, L Santen, A Schadschneider, and M Schreckenberg. Jamming transition in a cellular automaton model for traffic flow. *Physical Review E*, 57(2):1309, 1998.

[13] Cornell CCSL. Universal robotic gripper based on the jamming of granular material playing at original volume. – YouTube. https://www.youtube.com/watch?v=bFW7VQpY-Ik. [Online; accessed 29-June-2017].

[14] Eric Brown, Nicholas Rodenberg, John Amend, Annan Mozeika, Erik Steltz, Mitchell R Zakin, Hod Lipson, and Heinrich M Jaeger. Universal robotic gripper based on the jamming of granular material. *Proceedings of the National Academy of Sciences*, 107(44):18809–18814, 2010.

[15] Gianfranco D'Anna and Gerard Grémaud. The jamming route to the glass state in weakly perturbed granular media. *Nature*, 413(6854):407, 2001.

[16] Salvatore Torquato and Frank H Stillinger. Multiplicity of generation, selection, and classification procedures for jammed hard-particle packings. *The Journal of Physical Chemistry B*, 105(47):11849–11853, 2001.

[17] Aleksandar Donev, Frank H Stillinger, PM Chaikin, and Salvatore Torquato. Unusually dense crystal packings of ellipsoids. *Physical review letters*, 92(25):255506, 2004.

[18] Salvatore Torquato, Thomas M Truskett, and Pablo G Debenedetti. Is random close packing of spheres well defined? *Physical review letters*, 84(10):2064, 2000.

[19] Peter Olsson and S Teitel. Critical scaling of shearing rheology at the jamming transition of soft-core frictionless disks. *Physical Review E*, 83(3):030302, 2011.

[20] Peter Olsson and S Teitel. Herschel-bulkley shearing rheology near the athermal jamming transition. *Physical review letters*, 109(10):108001, 2012.

[21] Peter Olsson. Relaxation times and rheology in dense athermal suspensions. *Physical Review E*, 91(6): 062209, 2015.

[22] Michael Plischke and Birger Bergersen. *Equilibrium statistical physics*. World Scientific Publishing Co Inc, 1994.

[23] Daniel Vågberg, Daniel Valdez-Balderas, MA Moore, Peter Olsson, and Stephen Teitel. Finite-size scaling at the jamming transition: Corrections to scaling and the correlation-length critical exponent. *Physical Review E*, 83(3):030303, 2011.

[24] Michio Otsuki and Hisao Hayakawa. Critical scaling near jamming transition for frictional granular particles. *Physical Review E*, 83(5):051301, 2011.

[25] Aleksandar Donev, Ibrahim Cisse, David Sachs, Evan A Variano, Frank H Stillinger, Robert Connelly, Salvatore Torquato, and Paul M Chaikin. Improving the density of jammed disordered packings using ellipsoids. *Science*, 303(5660):990–993, 2004.

[26] Pinaki Chaudhuri, Ludovic Berthier, and Srikanth Sastry. Jamming transitions in amorphous packings of frictionless spheres occur over a continuous range of volume fractions. *Physical review letters*, 104(16): 165701, 2010.

[27] AW Lees and SF Edwards. The computer study of transport processes under extreme conditions. *Journal of Physics C: Solid State Physics*, 5(15):1921, 1972.

[28] Gary P Morriss and Denis J Evans. *Statistical Mechanics of Nonequilbrium Liquids*. ANU Press, 2013.

[29] Loic Vanel, Daniel Howell, D Clark, RP Behringer, and Eric Clément. Memories in sand: Experimental tests of construction history on stress distributions under sandpiles. *Physical Review E*, 60(5):R5040, 1999.

[30] Masahiro Toiya, Justin Stambaugh, and Wolfgang Losert. Transient and oscillatory granular shear flow. *Physical review letters*, 93(8):088001, 2004.

[31] Donald W Marquardt. An algorithm for least-squares estimation of nonlinear parameters. *Journal of the society for Industrial and Applied Mathematics*, 11(2):431–441, 1963.

[32] William H Press. *Numerical recipes 3rd edition: The art of scientific computing*. Cambridge university press, 2007.

[33] William H Press, Saul A Teukolsky, William T Vetterling, and Brian P Flannery. *Numerical recipes in C*, volume 2. Cambridge university press Cambridge, 1996.

[34] DJ Durian. Foam mechanics at the bubble scale. *Physical review letters*, 75(26):4780, 1995.

[35] Daniel Vågberg, Peter Olsson, and S Teitel. Universality of jamming criticality in overdamped shear-driven frictionless disks. *Physical review letters*, 113(14):148002, 2014.

[36] Daniel Vågberg, Peter Olsson, and S Teitel. Universality of jamming criticality in overdamped shear-driven frictionless disks – Supplemental material. *Physical review letters*, 113(14):148002, 2014.

[37] Aleksandar Donev, Robert Connelly, Frank H Stillinger, and Salvatore Torquato. Underconstrained jammed packings of nonspherical hard particles: Ellipses and ellipsoids. *Physical Review E*, 75(5):051304, 2007.

[38] Daniel Vågberg, Peter Olsson, and S Teitel. Shear banding, discontinuous shear thickening, and rheological phase transitions in athermally sheared frictionless disks. *Physical Review E*, 95(5):052903, 2017.

[39] Carl F Schreck, Ning Xu, and Corey S O'Hern. A comparison of jamming behavior in systems composed of dimer-and ellipse-shaped particles. *Soft Matter*, 6(13):2960–2969, 2010.

[40] Daniel Vågberg, Peter Olsson, and S Teitel. Dissipation and rheology of sheared soft-core frictionless disks below jamming. *Physical Review Letters*, 112(20):208303, 2014.

[41] Corey S O'Hern, Stephen A Langer, Andrea J Liu, and Sidney R Nagel. Random packings of frictionless particles. *Physical Review Letters*, 88(7):075507, 2002.

[42] Aleksandar Donev. *Jammed Packings of Hard Particles*. PhD thesis, Princeton University, September 2006. http://cims.nyu.edu/~donev/Thesis.pdf.

A | Elastic force between ellipsoids

A.1 Reduced belonging matrix

An ellipsoid $\mathcal{A}$ of centre $\vec{v}$ and semi-axes $(R_i)_{i=1:3}$ can be described by the matrix

$$\bar{B}(O,(R_i)_{i=1:3}) \equiv O\text{diag}(R_i^{-2})_{i=1:3}O^T \tag{A.1}$$

where O is the symmetric rotation matrix corresponding to the change of basis from the ellipsoid frame to the reference frame, such as

$$\forall \vec{r} \in \mathbb{R}^3, \begin{cases} (\vec{r}-\vec{v})^T\bar{B}(\vec{r}-\vec{v}) < 1 & \text{if } \vec{r} \in \mathcal{A} \setminus \bar{\mathcal{A}} \\ (\vec{r}-\vec{v})^T\bar{B}(\vec{r}-\vec{v}) = 1 & \text{if } \vec{r} \in \bar{\mathcal{A}} \\ (\vec{r}-\vec{v})^T\bar{B}(\vec{r}-\vec{v}) > 1 & \text{if } \vec{r} \notin \mathcal{A} \end{cases} \tag{A.2}$$

and with which we can write

$$\mu^2(\vec{r} \in \mathbb{R}^3) = (\vec{r}-\vec{v})^T\bar{B}(O,(R_i)_{i=1:3})(\vec{r}-\vec{v}) \tag{A.3}$$

where $\mu(\vec{r})$ is the rescaling factor that has to be applied to the axes of $\mathcal{A}$ for $\vec{r}$ to be on its surface.

For simplicity, we will write $\bar{B}_{\mathcal{A}} \equiv \bar{B}(O,(R_i)_{i=1:3})$.

We have for all $\vec{r}$ on the surface of $\mathcal{A}$ that $\mu^2(\vec{r}) = 1$, therefore the surface of $\mathcal{A}$ is an isosurface of μ^2. Therefore, we can conclude that the vector

$$\vec{\nabla}\mu^2(\vec{r}) = 2\bar{B}_{\mathcal{A}}(\vec{r}-\vec{v}) \tag{A.4}$$

is orthogonal to the surface of $\mathcal{A}$ in $\vec{r}$.

A.2 Force

We assumed that the force exerted on an ellipsoid $\mathcal{A}$ by an ellipsoid $\mathcal{B}$ of centre $\vec{r}_{\mathcal{A}}$ and $\vec{r}_{\mathcal{B}}$ respectively is

$$\vec{f}^{\text{el}}_{\mathcal{AB}}(\vec{r_{\mathcal{A}}},\vec{r_{\mathcal{B}}}) = k_e(1-\mu(\vec{r_{\mathcal{A}}},\vec{r_{\mathcal{B}}}))\frac{d\mu}{d\vec{r_{\mathcal{A}}}}(\vec{r_{\mathcal{A}}},\vec{r_{\mathcal{B}}}) \tag{A.5}$$

according to equation 1.26, where $\mu(\vec{r}_{\mathcal{A}},\vec{r}_{\mathcal{B}})$ is the rescaling factor that has to be applied to both $\mathcal{A}$ and $\mathcal{B}$ for them to be externally tangent.

Contrarily to the case of spheres, we have for ellipsoids that the rescaling factor $\mu(\vec{r_{\mathcal{A}}},\vec{r_{\mathcal{B}}})$ is not uniquely determined by the positions of their centres. Indeed, if we were to add $d\vec{r_{\mathcal{A}}}$ to the position $\vec{r_{\mathcal{A}}}$ of the centre of ellipsoid $\mathcal{A}$, the contact point $\vec{r_C}$ with ellipsoid $\mathcal{B}$ would move as well.

Since we are looking for the first derivative of the quantity $\mu(\vec{r_{\mathcal{A}}},\vec{r_{\mathcal{B}}})$, we will approximate rescaled ellipsoids by their respective tangent planes at $\vec{r_C}$ as suggested by [42].

If ellipsoid $\mathcal{A}$ is moved by $d\vec{r_{\mathcal{A}}}$, there appears a gap dh between the tangent planes of the rescaled ellipsoids with

$$dh = d\vec{r_{\mathcal{A}}} \cdot \vec{n}_{\mathcal{A}}(\vec{r_C}) \tag{A.6}$$

where $\vec{n}_{\mathcal{A}}(\vec{r_C})$ is the outward-facing unitary surface vector of ellipsoid $\mathcal{A}$ in $\vec{r_C}$.

To close this gap, we have to rescale the – yet rescaled – ellipsoids with a factor ν so that

$$((\vec{r_C}-\vec{r_{\mathcal{A}}})-\nu(\vec{r_C}-\vec{r_{\mathcal{A}}}))\cdot\vec{n}_{\mathcal{A}}(\vec{r_C}) - ((\vec{r_C}-\vec{r_{\mathcal{B}}})-\nu(\vec{r_C}-\vec{r_{\mathcal{B}}}))\cdot\vec{n}_{\mathcal{A}}(\vec{r_C}) = dh \Rightarrow 1-\nu = \frac{dh}{(\vec{r_{\mathcal{B}}}-\vec{r_{\mathcal{A}}})\cdot\vec{n}_{\mathcal{A}}(\vec{r_C})}$$

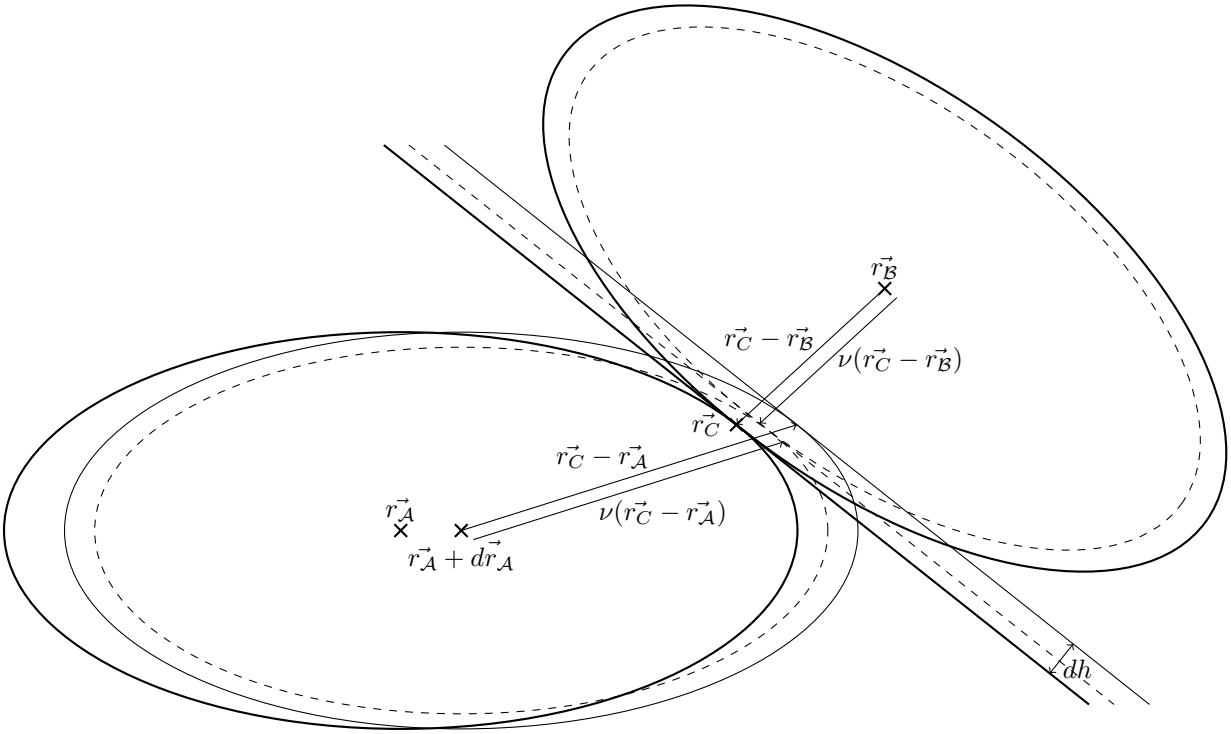

Figure A.1: Ellipsoids rescaled with rescaling factor $\mu(\vec{r_{\mathcal{A}}}, \vec{r_{\mathcal{B}}})$ and their contact plane in plain thick trait. Ellipsoids rescaled with rescaling factor $\mu(\vec{r_{\mathcal{A}}} + \vec{dr_{\mathcal{A}}}, \vec{r_{\mathcal{B}}})$ and their contact plane in dashed trait.

and

$$\mu(\vec{r_{\mathcal{A}}} + \vec{dr_{\mathcal{A}}}, \vec{r_{\mathcal{B}}}) = \nu\mu(\vec{r_{\mathcal{A}}}, \vec{r_{\mathcal{B}}}) \Rightarrow \vec{dr_{\mathcal{A}}} \cdot \frac{d\mu}{\vec{dr_{\mathcal{A}}}}(\vec{r_{\mathcal{A}}}, \vec{r_{\mathcal{B}}}) = -\mu(\vec{r_{\mathcal{A}}}, \vec{r_{\mathcal{B}}})(1-\nu)$$

which, with equation A.6, leads to

$$\frac{d\mu}{\vec{dr_{\mathcal{A}}}}(\vec{r_{\mathcal{A}}}, \vec{r_{\mathcal{B}}}) = -\mu(\vec{r_{\mathcal{A}}}, \vec{r_{\mathcal{B}}}) \frac{\vec{n}_{\mathcal{A}}(\vec{r_C})}{(\vec{r_{\mathcal{B}}} - \vec{r_{\mathcal{A}}}) \cdot \vec{n}_{\mathcal{A}}(\vec{r_C})}$$

We can then conclude, with equation **??**, that

$$\frac{d\mu}{\vec{dr_{\mathcal{A}}}}(\vec{r_{\mathcal{A}}}, \vec{r_{\mathcal{B}}}) = -\frac{\mu(\vec{r_{\mathcal{A}}}, \vec{r_{\mathcal{B}}})}{(\vec{r_{\mathcal{B}}} - \vec{r_{\mathcal{A}}})^T \bar{B}_{\mathcal{A}}(\vec{r_C} - \vec{r_{\mathcal{A}}})} \bar{B}_{\mathcal{A}}(\vec{r_C} - \vec{r_{\mathcal{A}}}) \tag{A.7}$$

Therefore, with equation 1.26, we finally have that

$$\boxed{\vec{f}^{\text{el}}_{\mathcal{AB}}(\vec{r_{\mathcal{A}}}, \vec{r_{\mathcal{B}}}) = -k_e \frac{\mu(\vec{r_{\mathcal{A}}}, \vec{r_{\mathcal{B}}})\,(1 - \mu(\vec{r_{\mathcal{A}}}, \vec{r_{\mathcal{B}}}))}{(\vec{r_{\mathcal{B}}} - \vec{r_{\mathcal{A}}})^T \bar{B}_{\mathcal{A}}(\vec{r_C} - \vec{r_{\mathcal{A}}})} \bar{B}_{\mathcal{A}}(\vec{r_C} - \vec{r_{\mathcal{A}}})} \tag{A.8}$$